

Non-Fermi liquid behavior of doped Kondo insulator: The unique properties of $\text{CeRhSb}_{1-x}\text{Te}_x$.

A. Ślebarski,^{1,2,3} J. Spałek,⁴ and M. Fijałkowski^{5,2}

¹*Institute of Low Temperature and Structure Research,
Polish Academy of Sciences, ul. Okólna 2, 50-422 Wrocław, Poland*

²*Centre for Advanced Materials and Smart Structures,
Polish Academy of Sciences, ul. Okólna 2, 50-422 Wrocław, Poland*

^{3*} *Author to whom correspondence should be addressed: andrzej.slebarski@us.edu.pl*

⁴*Institute of Theoretical Physics, Jagiellonian University, ul. Łojasiewicza 11, 30-348 Kraków, Poland*

⁵*Institute of Physics, University of Silesia in Katowice,
ul. 75 Pułku Piechoty 1, 41-500 Chorzów, Poland*

It follows from our analysis of CeRhSb that the formation of Kondo insulator state due to the presence of the collective spin singlet state is strongly reduced by its doping with various dopants when their amount exceeds 8–10%, regardless of whether they are substituted for Ce, Rh or Sb. A wide variety of experimental results (electrical resistivity ρ , magnetic susceptibility χ , specific heat C , x-ray photoelectron spectroscopy) and theoretical investigations have convincingly demonstrated the proposed earlier scaling law $\chi \times \rho = \text{const.}$ in the Kondo insulator regime, which is universal for all known Kondo insulators. We also analyze the properties of the Griffiths-phase for CeRhSb when Pd substitutes Rh, or Sb is fractionally replaced by Te and Sn, whereas doping of Ce with La leads to the formation of magnetic cluster structure as a result of the Kondo hole effect. Magnetoresistance of CeRhSb and $\text{CeRhSb}_{0.98}\text{Te}_{0.02}$ as a function of the field B shows a $-B^2$ behavior, which provides evidence for the topologically nontrivial nature of these compounds, as was previously predicted theoretically for CeRhSb on the basis on the band structure calculations.

I. INTRODUCTION

The stoichiometric CeRhSb Kondo insulator (KI) belongs to the class of strongly correlated materials with the small-gap $\Delta \sim 8$ K semiconducting properties and a heavy-fermion metallic state, setting in gradually at elevated temperature $T \geq \Delta$ [1]. Within the framework of the periodic Anderson model, the gap arises from the strongly renormalized by electronic correlations and hybridization V between the conduction band and the strongly correlated f -electron states. Moreover, Δ is strongly temperature dependent [2, 3], in contrast to usual narrow-gap semiconductors. A full understanding of KIs is in part obscured by the circumstance that relatively small values of both magnetic susceptibility χ and the gap when $T \rightarrow 0$ lead to their properties alteration by a minute content of magnetic or other impurities [4–6]. In effect, it is often difficult to differentiate between the intrinsic and extrinsic properties of these systems. It has been shown that even a relatively small number of in-gap states due to the lattice defects or doping plays a destructive role in the formation of the Kondo insulating ground state, manifested, e.g., in resistivity ρ through its deviation from the activated behavior at the lowest temperatures. Here we show that the atomic disorder, resulting from lattice defects in parent CeRhSb or generated by doping, can lead to local magnetic inhomogeneities, characteristic of the onset of the Griffiths phase.

For the last two decades, an increasing attention has been devoted to Kondo insulators due to the fact that they can also become topological Kondo insulators (TKI), as they possess that extremely narrow energy gap. One of the first arguments was the observation of devi-

ation from activated behavior of resistivity at the lowest temperatures $T \ll \Delta$. The first theoretically predicted TKI was SmB_6 [7, 8]. The metallic surface states have been documented by angle-resolved photoemission spectroscopy (ARPES) [9–11] and electrical transport measurements [12–14], providing an evidence for SmB_6 as a possible TKI. It has also been predicted theoretically that CeNiSn [15] and CeRhSb [16] may be regarded as novel topological Kondo insulators possessing Möbius-twisted surface states. These materials were classified as the Kondo insulators with the gap that closes along a axis [17]. In effect, CeNiSn and CeRhSb have been termed as *failed Kondo insulators* [15] with a pseudogap. But, the topological Fermi-surface features have not been confirmed experimentally as yet [18]. We observe a negative magnetoresistance MR with quadratic field dependence for CeRhSb which may indicate the chiral magnetic behavior, suggesting the topologically nontrivial electronic state of that material.

The structure of this paper is as follows. After Introduction and Experimental Details (Secs. I and II, respectively), in Sec. III, we specify, on the example of $\text{CeRh}_{1-x}\text{Pd}_x\text{Sb}$, the critical doping x , at which the collective Kondo spin-singlet state (KI regime) transforms into metallic (non-KI) state (cf. Fig. 5). For reference, we also specify there first the detailed resistivity behavior (cf. Fig 6), and magnetic crossover from anomalous to Curie-Weiss regime (cf. Figs. 2 and 3). This anomalous magnetic behavior is compared with the calculated temperature behavior of a canonical Kondo insulator (cf. also Appendix A for some theoretical details). On the basis of electrical resistivity $\rho(T)$ scaling, we have determined the anomalous applied field scaling of the pseudogap Δ

for $\text{CeRhSb}_{1-x}\text{Te}_x$, as well as the temperature scaling of the magnetic susceptibility χ and relative specific heat C/T (cf. Figs. 7-9, respectively). The data extrema are associated with the onset of Griffiths phase in the temperature range $T \sim 1$ K. All of them provide further evidence for non-KI behavior for $\text{CeRhSb}_{1-x}\text{Te}_x$. The data presented in Sec. IIIC elaborate on the details of the proposed non-KI scenario. The discussed data in Sec. IIIA–C have provided novel scaling laws accumulated in Table I. Finally, Sec. IV contains a brief recapitulation of our analysis.

II. EXPERIMENTAL DETAILS

Polycrystalline samples of $\text{Ce}_{1-x}\text{La}_x\text{RhSb}$, $\text{CeRh}_{1-x}\text{Pd}_x\text{Sb}$, $\text{CeRhSb}_{1-x}\text{Sn}_x$, and $\text{CeRhSb}_{1-x}\text{Te}_x$ were prepared via arc melting. For the first three series mentioned, pure CeRhSb and respectively LaRhSb (ϵ -TiNiSi-type structure, space group $Pnma$), CePdSb (CaIn_2 -type structure, space group $P6_3/mmc$ [19, 20]), or CeRhSn (Fe_2P -type structure, space group $P6_2m$ [21]) were the first arc melted, and then the respective diluted alloys were prepared by mixing the nominal compositions of the master compounds. CeRhTe is, however, not formed, therefore the stoichiometric amounts of the constituent elements were arc melted for $\text{CeRhSb}_{1-x}\text{Te}_x$. To ensure homogeneity, each sample was turned over and remelted several times and then annealed at 800 °C for 2 weeks. An excess amount of 1% Sb was added to compensate for losses of this metal within the melting process. The crystal structure of the annealed samples was checked by powder x-ray diffraction. The Rietveld structural refinement revealed that the samples crystallize with orthorhombic the ϵ -TiNiSi structure (space group $Pnma$) and are obtained as single phases in a limited concentration $x < \sim 0.1$ range. The series of $\text{CeRhSb}_{1-x}\text{Te}_x$ samples have not been known and investigated so far. The single-phase components of the series were obtained for $x < 0.08$. The x-ray diffraction pattern of $\text{CeRhSb}_{0.98}\text{Te}_{0.02}$ is shown in Fig. 1.

The ac electrical resistivity ρ and ac magnetic susceptibility χ_{ac} measurements were performed using the quantum design (QD) PPMS platform. The resistivity and specific heat was measured in the temperature range 0.4 – 300 K and in external magnetic fields up to 9 T also using QD PPMS platform. dc magnetic susceptibility and the magnetization measurements were carried out using a commercial QD SQUID magnetometer in the magnetic field up to 7 T.

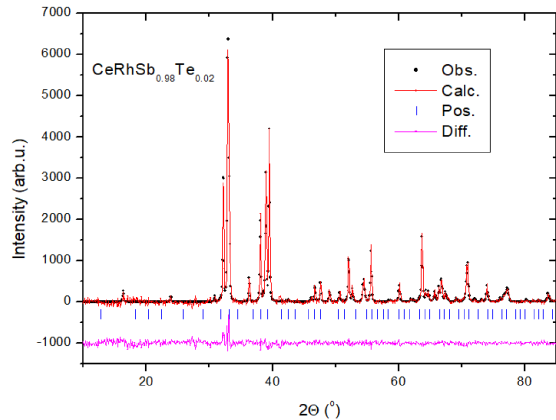


FIG. 1. Powder XRD pattern of $\text{CeRhSb}_{0.98}\text{Te}_{0.02}$ recorder at room temperature. The solid red line (Calc.) through the experimental points (black points - Obs.) is a calculated Rietveld refinement profile. The lowest curve (Diff.) represents the difference between the experimental and calculated results. The vertical bars (Pos) indicate the Bragg positions for the ϵ -TiNiSi-type structural model. The weighted profile R_{wp} factor is 3.2%, $R_{exp} = 3.0\%$, and the lattice parameter $a = 7.4265(2)$ Å (7.4130 Å), $b = 4.6199(0)$ Å (4.6124 Å), and $c = 7.8604(3)$ Å (7.8531 Å) are compared with the lattice parameters of CeRhSb (in the brackets). The meaning of R is defined, e.g., in Ref. [22].

III. INTERPLAY BETWEEN SPIN-GLASS-LIKE AND KONDO INSULATING STATE: THE CASE OF LOCAL DISORDER IN CeRhSb

A. Universal scaling law: $\chi(T)\rho(T) = \text{const.}$

Our earlier research on CeRhSb [23], $\text{CeRhSb}_{1-x}\text{Sn}_x$ [24, 25], CeNiSn [26], and $\text{CeNi}_{1-\delta}\text{Sn}_{1+\delta-x}\text{Sb}_x$ [27], as well as that on $\text{Ce}_3\text{Bi}_4\text{Pt}_3$ [28, 29] and FeSi [28, 30] follow that the Kondo insulating state can be characterized by the following features: (i) The number of valence electrons is even, i.e., it is 18 for CeRhSb and CeNiSn (including one 4f electron due to Ce), whereas $\text{Ce}_3\text{Bi}_4\text{Pt}_3$ has 54 such electrons and FeSi has 12. Based on that fact one can expect the complete screening of the atomic moment of either Ce^{3+} or Fe^{4+} ions within the formula unit if the coupling of the surrounding screening carriers has an antiferromagnetic character. (ii) The resistivity $\rho(T)$ is thermally activated in the limited temperature range with a small activation gap, $\Delta \sim (1 - 10)$ meV. However, the gap is sometimes not easy to detect as the shallow impurity in-gap states form an impurity band, overlapping with the upper and/or the lower hybridized band, thus leading to a semimetallic behavior. (iii) The narrow gap or pseudogap is associated with the collective Kondo spin-singlet state formation, singled out directly by the decreasing magnetic susceptibility $\chi(T)$ when $T \rightarrow 0$, provided such a system does not order magnetically. In that case, the impurity contribution must be singled out and properly subtracted. Also, the disorder

creates localized states in the pseudogap region and leads to a magnetic glassy state, which gives rise to the Curie-Weiss contribution $y \frac{C}{T - \theta_{CW}}$ to $\chi(T)$ at the lowest temperatures with $y \sim 0.01$, as well as removes the activated behavior when the dopant content is $x > \sim 0.08$. (iv) The resistivity and magnetic susceptibility obey [24] a simple scaling law $\chi(T)\rho(T) = const.$, particularly in the regime $k_B T < \Delta$, when the number of excited carriers is small. The scaling law $\chi\rho = const.$ is universal for the known Kondo insulators, provided that impurity contribution is properly subtracted, see e.g., Refs. [24, 26, 28]. It is worth noting that for CeRhSb of very high purity [31] the susceptibility rapidly decreases in the KI regime and exhibits a clear $\chi \rightarrow 0$ behavior for $T \rightarrow 0$, cf., Ref. [24]. The scaling $\chi(T)\rho(T) = const.$ is the most char-

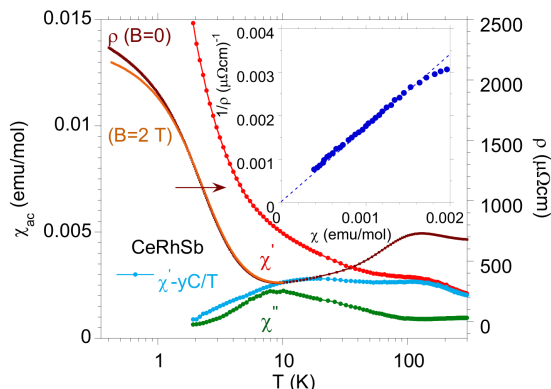


FIG. 2. Temperature dependence of the real (χ' , red points) and imaginary (χ'' , green points) components of ac magnetic susceptibility for CeRhSb ($\nu = 1$ kHz, amplitude of the magnetic field $B = 2$ G). The blue points represent $\chi'(T)$ subtracted by the Curie-Weiss contribution $y \frac{C}{T - \theta_{CW}}$, where $y = 0.028$ and $\theta_{CW} = 0.3$ K are from the best fit of C-W expression to χ' for $T < 100$ K. The brown and yellow points show the resistivity for CeRhSb at $B = 0$ and 2 T, respectively. The inset demonstrates the linear scaling law between $\chi' - yC/T$ and $1/\rho$ in the temperature range ($1.8 < T < 5$) K.

acteristic behavior. Therefore, we discuss first the full-gap semiconductor CeRhSb with the conductivity gap $\Delta = 6$ K, obtained from fitting of the resistivity data to $\rho \sim e^{\Delta/k_B T}$ law. The scaling law $\chi(T)\rho(T) = const.$ shown in the inset to Fig. 2 is clearly obeyed. Additionally, the displayed there χ'' component exhibits a broad maximum at ~ 9 K, which indicates both the presence of the hybridization gap and of a very weak inhomogeneous spin-glass-like ground state. When the number of local defects increases, e.g., due to doping, then χ_{ac} is both frequency (ν) and field dependent [23], as shown in Fig. 3 for the Kondo-hole $\text{Ce}_{0.98}\text{La}_{0.02}\text{RhSb}$ semimetal. In the case of the increased number of structural defects, the scaling $\chi\rho = const.$ is practically impossible to be identified and is due to the presence of a glassy phase, which represents a strong disturbance of the paramagnetic KI ground state in this case.

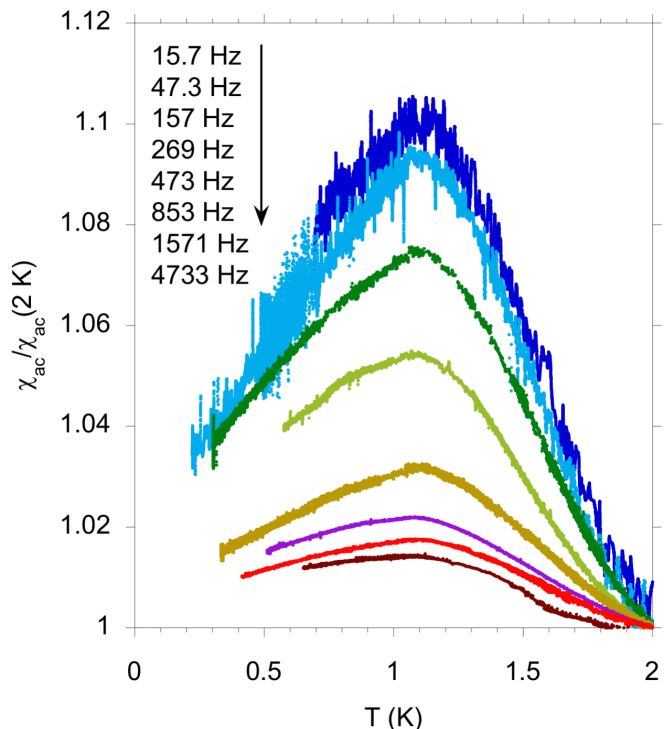


FIG. 3. Low-temperature ac magnetic susceptibility for $\text{Ce}_{0.98}\text{La}_{0.02}\text{RhSb}$, measured at different frequencies ν under magnetic field of 2 G. The data are normalized χ_{ac} at 2 K, respectively (taken from Ref. [23]).

B. Nonmagnetic Kondo-compensated state in the case with intraatomic hybridization: The $\chi \rightarrow 0$ for $T \rightarrow 0$ behavior within the periodic Anderson-Kondo model

To set a reference point for further discussion we have provided in Fig. 4 temperature dependence of the static magnetic susceptibility obtained theoretically for nonmagnetic KI [32]. The calculation involved an intraatomic hybridization V , as well as have been carried out for a number of electrons $n_e = 2$ per site, the position of the f -level $\epsilon_f = -0.85$, and the $f-f$ Hubbard interaction magnitude $U = 2$ (all parameters are in units of bare conduction-band bandwidth W). We see that for the even number of electrons the susceptibility $\chi_m \rightarrow 0$ with $T \rightarrow 0$, with T^2 dependence as for Landau Fermi liquid, whereas it takes the standard Curie-Weiss form in the high-temperature limit (cf. insets). Also, a broad maximum is observed around temperature $V^2/U \sim 0.05W$, characteristic of a gradual transition from the Fermi-liquid (FL) to the f -electron localized moment (LM) state (with the f -level occupancy $n_f \rightarrow 1$ in the latter limit).

All these features, together with the universal scaling law $\chi_m \times \rho = const.$, proposed and experimentally documented earlier [24, 25, 28], provide us with the confidence that our method of approach describes properly the the universal trend of the experimental data for KI systems.

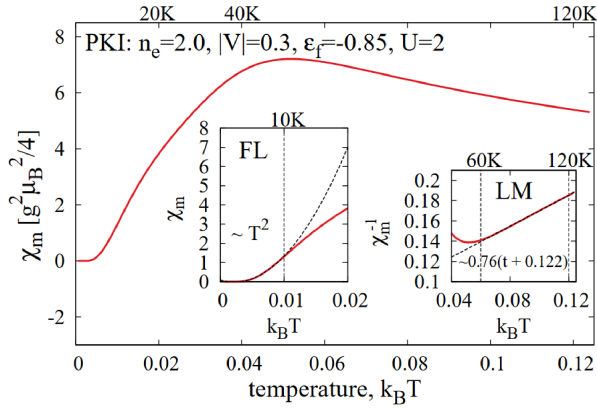


FIG. 4. Temperature dependence of the zero-field magnetic susceptibility for the nonmagnetic Kondo insulator (PKI). The insets show PKI evolution from the Fermi-liquid regime (FL), to the localized moment regime (LM). The upper-temperature scale is provided for bare conduction bandwidth $W = 103$ K (taken from Refs. [32, 66]; for details see Appendix A).

C. Non-Fermi-liquid behavior in CeRhSb with dopants: Griffiths phase in CeRhSb_{1-x}Te_x, CeRh_{1-x}Pd_xSb and Ce_{0.98}Th_{0.02}Sb

Doping of CeRhSb, regardless of whether the Ce, Rh or Sb atoms are replaced with another atom M , causes the parent system ceases to be a single phase already for the impurity concentration x larger than about 15–20%. For the systems investigated so far Ce_{1-x}M_xRhSb ($M = \text{La}$ [23, 33, 34] or Th [35]), CeRh_{1-x}M_xSb ($M = \text{Pd}$ [36, 37]), or CeRhSb_{1-x}Sn_x [21, 23–25], there is a critical concentration of x_{cr} for each of them, which separates the Kondo-insulator phase from the metallic one. The reason for the transformation KI→metal with increasing x is formation of partially filled hybridized band above critical concentration x_{cr} as shown in Fig. 5 for the CeRh_{1-x}Pd_xSb alloys (for details, see Ref. [37]). This transformation was predicted theoretically [38] and has been documented experimentally [23, 37]. The effect is not dependent on whether the doping generates a Kondo hole (La, Th dopants) and is neither associated with an increasing (Pd, Te, dopants) nor with decreasing (Sn dopant) a number of carriers. Here we analyze the impact of Te for Sb substitution on the hybridized structure formation. Namely, we document experimentally that the Te impurities (when $x < 0.08$) generate the Griffiths-type phase as a result of doping-induced lattice disorder. Intriguingly, we observe a similar Griffiths-type phase in CeRhSb doped by various other M dopants. Below we present some of those examples. First, we present the magnetic and electrical transport data for CeRhSb with Sb substituted by Te, i.e., for CeRhSb_{0.98}Te_{0.02}. Figure 6 exhibits low-temperature electrical resistivity ρ

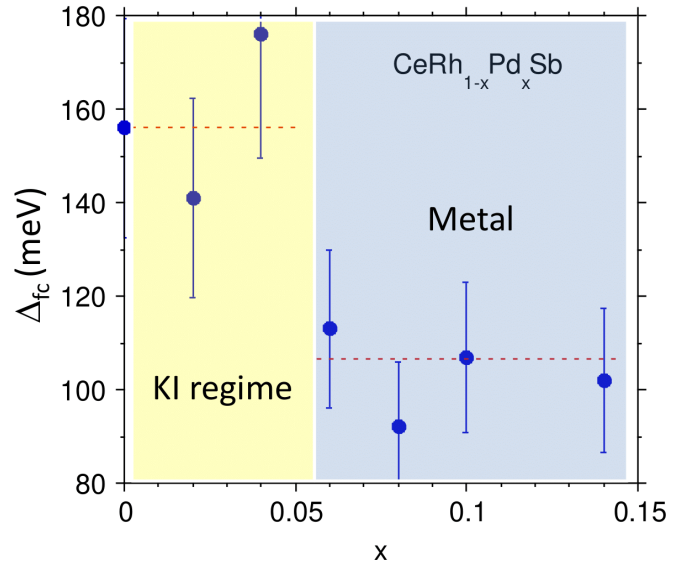


FIG. 5. CeRh_{1-x}Pd_xSb: hybridization energy $\Delta_{fc} = \pi V^2 N(\epsilon_F)$ [39] vs x obtained from the Ce 3d XPX spectra based on the Gunnarsson and Schönhammer theoretical model [40], V is a matrix element of mixing between $4f$ and conduction electrons at the Fermi level, ϵ_F , and $N(\epsilon_F)$ is the density of states at ϵ_F .

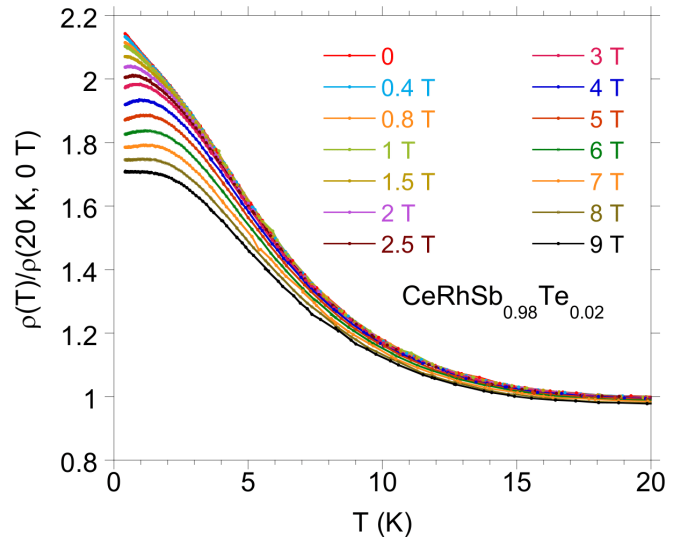


FIG. 6. CeRhSb_{0.98}Te_{0.02}. The low-temperature electrical resistivity $\rho(T)$, normalized to $\rho = 262 \mu\Omega\text{cm}$, at $T = 20$ K and $B = 0$, $\rho(T)/\rho(T = 20\text{K})$, for different magnetic field values.

at different magnetic fields for CeRhSb_{0.98}Te_{0.02}. The curves show a well-defined thermally activated behavior, where $\rho \sim \exp(\Delta/T)$ in the low-temperature regime that is characteristic of a nondegenerate semiconductor with activated energy $\Delta(B)$, shown in Fig. 7. We should also note that: (i) an increase in ρ generated by a KI (pseudo)gap decreases systematically with increasing x , (ii) the magnetic field leads to the saturation of ρ at the

lowest temperatures $T < \sim 2$ K, and finally (iii) in the applied field up to 9 T the CeRhSb gap is reduced to its of 95% value of $\Delta(0)$, whereas the doping leads to stronger field reducing of Δ , as illustrated in Fig. 7. However, the field influence is not x -dependent and is weaker than expected.

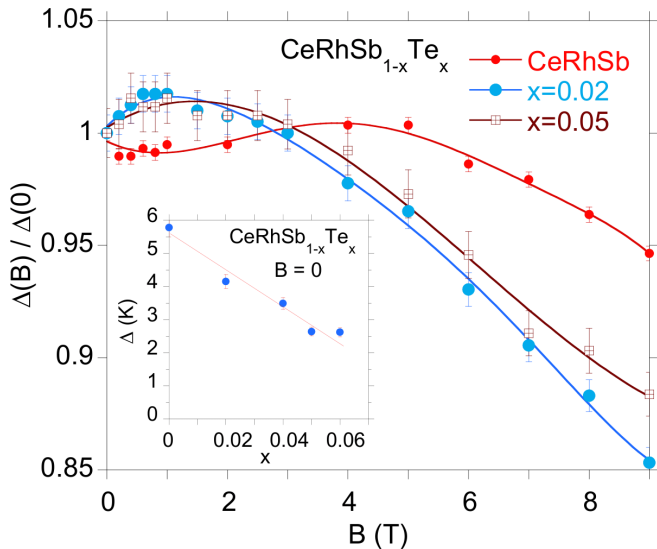


FIG. 7. CeRhSb_{0.98}Te_{0.02}; the KI gap $\Delta(B)$ as a function of applied magnetic field for components $x = 0.02$ and 0.05 in comparison to the change of $\Delta(B)$ for parent compound CeRhSb. The inset displays the change of Δ with x under zero magnetic field.

Low temperature magnetic susceptibility and C/T data for CeRhSb_{1-x}Te_x compounds ($x = 0.02, 0.03$, and 0.05) are plotted on a double logarithmic scale in Fig. 8(a). Both $\chi \sim T^{-1+\lambda}$ and $C/T \sim T^{-1+\lambda}$ (b) follow a power-law temperature dependence with similar λ , as shown in Table I. The observed power law dependencies $\chi \sim T^{-1+\lambda}$ and $C/T \sim T^{-1+\lambda}$, and the required agreement between λ s from $C(T)/T$ and $\chi(T)$ data support the Griffiths phase model [41]. Moreover, magnetization as a function of field up to 7 T does follow the predicted Griffiths phase behavior $\sigma \sim B^\lambda$ [42], as shown in Fig. 9 and in Table I. Note that λ from the best fit of expression $\sigma = \sigma(0) + mB^\lambda$ to the isotherms $\sigma_T(B)$, is temperature dependent and decreases with $T \rightarrow 0$; the correct value of λ is approximated by the $T = 0$ value.

Likewise, Griffiths phase behavior has been previously documented for Ce_{0.98}Th_{0.02}RhSn ([35], Table I), and for the series of CeRh_{1-x}Pd_xSb compounds (see Fig. 10, Table I). Ce_{0.98}Th_{0.02}RhSn shows a non-Fermi-liquid behavior in the specific heat within two decades of temperature [35], which is consistent with a quantum critical point scenario. However, the low temperature specific heat divided by temperature, C/T , of Ce_{0.98}Th_{0.02}RhSn can also be fit to a $T^{-1+\lambda}$ temperature dependence, which is consistent with the Griffiths phase disorder theory. Simultaneously, the low- T magnetic susceptibility can also be expressed as a power law with similar expo-

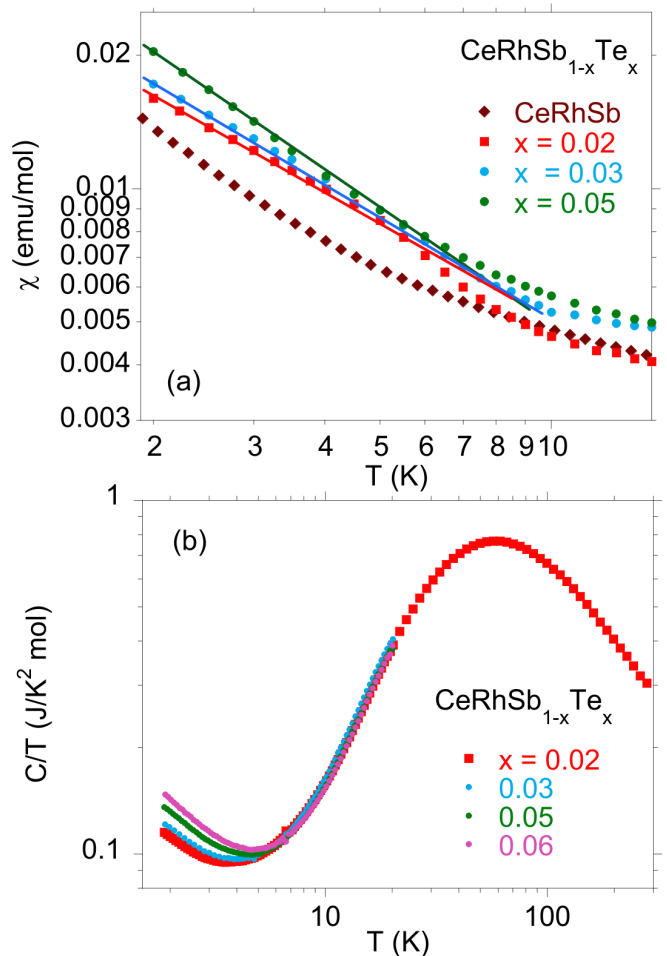


FIG. 8. CeRhSb_{0.98}Te_{0.02}: low temperature magnetic susceptibility (dc) vs T in log-log scale (a) and the specific heat divided by temperature, C/T , in log-log scale. Both quantities for $x = 0.02, 0.03, 0.05$, and 0.06 show a singular behavior at the low- T region.

nent λ in a temperature range 0.15 K – 10 K in agreement with the Griffiths phase model, and magnetization $\sigma \sim B^\lambda$. Note that the magnetization curves differ from a metamagnetic-like behavior of typical heavy fermion system [43]. It is intriguing to observe that this is an additional feature, by which KIs can be differentiated from the standard metallic heavy fermions. Ce_{1-x}Th_xRhSn samples with $x = 0.3$ and 0.4 were reported as magnetic, with spin cluster freezing below ~ 0.3 K [35]. Similar magnetic Kondo-insulator instabilities were predicted theoretically for the Kondo-hole systems, where they give rise to a bound state in the gap, leading to a Stoner-like ferromagnetic instability (cf., [44–46]). The Th and La impurities in CeRhSb are also regarded as Kondo holes. Clusters of Kondo holes have been studied in Ref. [23]. Evidence of the spin-glass-like behavior is shown in Fig. 3 for CeRhSb doped with La. Figure 11(a) shows the spin-glass-like contribution to the low-temperature specific heat C/T , obtained for the series of Ce_{1-x}La_xRhSb

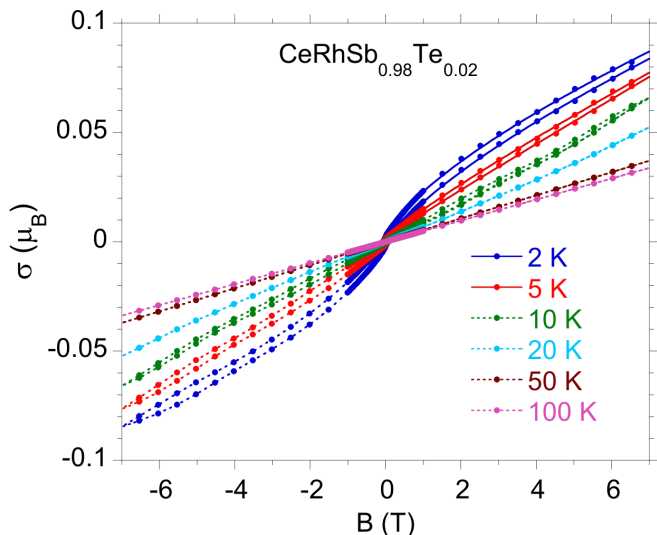


FIG. 9. Magnetization σ of $\text{CeRhSb}_{0.98}\text{Te}_{0.02}$ as a function of magnetic field, showing a hysteretic loop at 2 K and 5 K, and power law behavior, $\sigma \sim B^\lambda$. For each temperature the σ isotherms were measured under increasing and decreasing fields between -9 T and +9 T. The best fit with $\lambda = 0.69$ is represented by the blue lines at $T = 2$ K. For 5 K isotherm the best fit (red lines) gives $\lambda = 0.95$. At the remaining temperatures ($T > 10$ K) the hysteretic loop was not observed (the dotted lines connect the experimental points of the σ isotherms).

samples at $B = 0$. Panel (b) shows the ac magnetic susceptibility $\chi'(T)$ measured at various frequencies ν . For La impurities χ' basically does not follow the power-law behavior, with exclusion of the samples with small La content, $x = 0.02$ and 0.04 , where the high frequency ($\nu = 10$ kHz) real component of χ_{ac} has a $\chi' \sim T^{-0.9}$ scaling between 1.9 K and 10 K [see Fig. 11(b), straight-line part]. The above described properties suggest high-frequency-induced fluctuations of the magnetic clusters which are blocked up below $T_f \sim 1$ K, as illustrated in Fig. 3. However, this is not the Griffiths-phase case, as shown in Fig. 11 $C \sim T^{3/2}$ for $T < T_f$, which could signal an appearance of an inhomogeneous magnetic state [47].

It is especially interesting when Sb in CeRhSb is partially substituted for Sn. This is the case with the decreasing number of valence electrons in the system $\text{CeRhSb}_{1-x}\text{Sn}_x$, when x increases. Previously [25], on the Sb-rich side ($0 \leq x \leq 0.2$, with $x = 0.2$ being the limit of solubility), we observe the transition KI \rightarrow NFL as a function of decreasing number of carriers. Namely, the system $\text{CeRhSb}_{1-x}\text{Sn}_x$ undergoes the Kondo insulator-weakly magnetic metal transformation via the quantum critical point (QCP) located at the critical concentration $x_{cr} \approx 0.12$. We have also observed an accompanying universal scaling $\chi\rho = \text{const.}$ in the quantum-coherence regime for $\text{CeRhSb}_{1-x}\text{Sn}_x$ with $x \leq 0.12$. In Table I we list the χ , σ and C parametrizations of $\text{CeRhSb}_{1-x}\text{Sn}_x$. For $x > x_{cr}$, these quantities fit the Griffiths-phase sce-

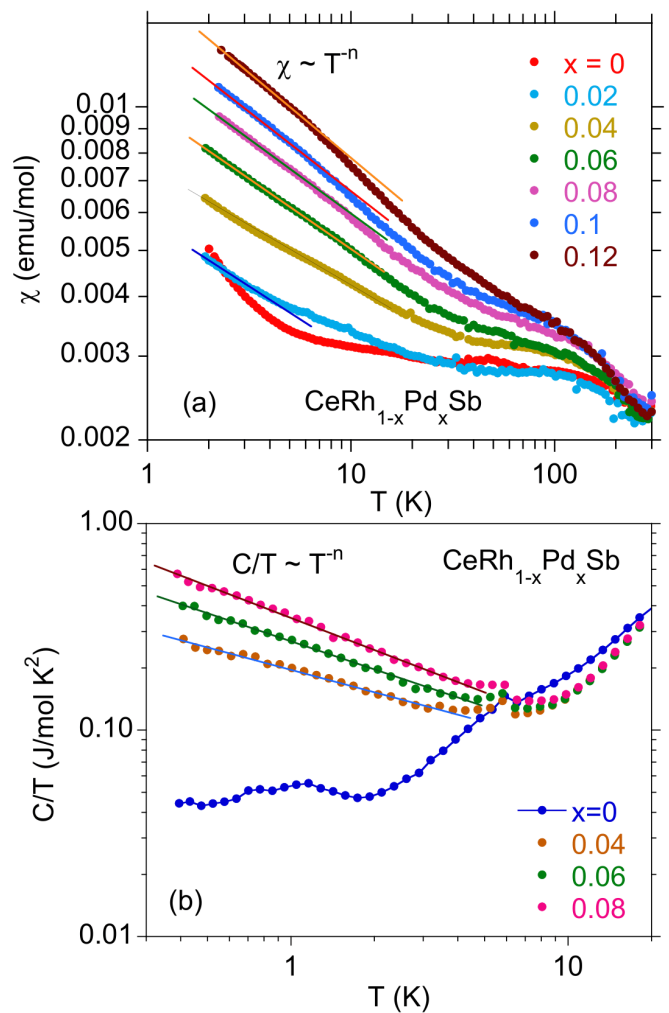


FIG. 10. $\text{CeRh}_{1-x}\text{Pd}_x\text{Sb}$; low temperature magnetic susceptibility (dc) vs T in log-log scale (a) and the specific heat divided by temperature, C/T , in log-log scale, with divergent behavior at the low- T region (b). A weak feature at 1.1 K in C/T of CeRhSb indicates on the weak magnetic inhomogeneity, due to strongly diluted magnetic entities (see text).

nario for a non-Fermi-liquid.

D. Magnetoresistance of CeRhSb and $\text{CeRhSb}_{0.98}\text{Te}_{0.02}$ Kondo insulators

Magnetoresistance, MR , of CeRhSb has been reported previously. However, the various measurements for obtaining the MR isotherms were limited only to low temperatures (1.3 K [49], 1.7 K [50]), and to the magnetic field up to 4.5 T at 4.2 K at various pressure [51], or were performed at 2 K, 4.5 K, and above 10 K under the increasing field with B increment every ~ 0.4 T up to 5.5 T [52]. Therefore, some interesting behaviors have been missed, especially in the T region of the KI gap, Δ . Here, we have measured carefully the MR isotherms of CeRhSb and $\text{CeRhSb}_{0.98}\text{Te}_{0.02}$ at temperatures below,

TABLE I. Specific heat C/T , d.c. magnetic susceptibility χ at 0.1 T, and magnetization σ parametrization of the results for $\text{Ce}_{1-x}\text{La}_x\text{RhSb}$, $\text{Ce}_{1-x}\text{Th}_x\text{RhSb}$ [35], $\text{CeRh}_{1-x}\text{Ni}_x\text{Sb}$ [48], $\text{CeRh}_{1-x}\text{Pd}_x\text{Sb}$ and $\text{CeRhSb}_{1-x}\text{Te}_x$ samples within KI regime ($\Delta > 0$). Susceptibility and specific heat, C/T , is fitted to a Griffiths phase scenario $\chi \sim C/T \sim T^n$, where $n = -1 + \lambda$, and $\sigma \sim B^\lambda$ [λ from $\sigma(B)$ isotherms is T dependent and decreases when $T \rightarrow 0$]. ^(a) A small La doping $x \geq 0.02$ of CeRhSb leads to formation of spin-glass-like state [23]. ^(b) $\text{CeRh}_{1-x}\text{Pd}_x\text{Sb}$, the χ , C/T , and σ data indicate a presence of very weak magnetic correlations for the components $x = 0.10$ and 0.12 . ^(c) Universal scaling law $\chi\rho = \text{const.}$ is documented for the components $x < 0.13$ of the series, after subtracting the impurity contribution $y\frac{C}{T}$ to $\chi(T)$, $y < 0.01$ (see Ref. [25]).

compound	x	$\chi \sim T^n$ $n = -1 + \lambda$	$C/T \sim T^n$ $n = -1 + \lambda$	$\sigma \sim B^\lambda$ λ
$\text{Ce}_{1-x}\text{La}_x\text{RhSb}$	$0 < x \leq 0.14^{(a)}$	not observed	not observed	
$\text{Ce}_{1-x}\text{Th}_x\text{RhSb}$ [35]	0.02	-0.36	-0.26	0.69 ($T = 2$ K)
	0.03	-0.39		
	0.04	-0.44		
		$T < 10$ K	$0.05 < T < 1.3$ K	
$\text{CeRh}_{1-x}\text{Ni}_x\text{Sb}$ [48]	0.05	-0.23		
	0.1	-0.22		
	$T < 15$ K			
$\text{CeRh}_{1-x}\text{Pd}_x\text{Sb}$	0.02	-0.27	-0.20	0.83 ($T = 2$ K)
	0.04	-0.27	-0.33	0.80 ($T = 2$ K)
	0.08	-0.32	-0.45	0.72 ($T = 2$ K)
	0.10 ^(b)	-0.38	-0.60	0.75 ($T = 2$ K)
	0.12 ^(b)	-0.36	-0.59	0.70 ($T = 2$ K)
		$T < 10$ K	$0.4 < T < 4$ K	
$\text{CeRhSb}_{1-x}\text{Te}_x$	0.02	-0.61	-0.45	0.69 ($T = 2$ K) ~ 0.44 ($T \rightarrow 0$)
	0.03	-0.65	-0.44	0.75 ($T = 2$ K) ~ 0.60 ($T \rightarrow 0$)
	0.04	-0.62	-0.52	0.70 ($T = 2$ K) ~ 0.55 ($T \rightarrow 0$)
	0.05	-0.70	-0.50	0.67 ($T = 2$ K) ~ 0.52 ($T \rightarrow 0$)
	0.06	-0.56	-0.53	0.53 ($T = 2$ K) ~ 0.45 ($T \rightarrow 0$)
		$T < 5$ K	$T < 3.2$ K	
$\text{CeRhSb}_{1-x}\text{Sn}_x$	$x \leq 0.12$	$\chi\rho = \text{const}^{(c)}$		
	0.13	-0.21	-0.33	0.71 ($T = 2$ K)
	0.14	-0.28		0.80 ($T = 2$ K)
	0.16	-0.10		0.78 ($T = 2$ K)
	0.19	-0.12		
		$T < 18$ K	$T < 4$ K	

as well as above Δ/k_B in the fields up to 9 T, with magnetic field sequence ($0 \rightarrow 9 \rightarrow -9 \rightarrow 0$) T, as shown in Figs. 12 and 13. First, we summarize the magnetoresistivity of parent CeRhSb : (i) Its MR isotherms at positive fields are in nature similar to those, reported

earlier, namely, at 2 K magnetoresistance in the increasing/decreasing directions of field sweeps shows a broad peak in the fields $B < 6$ T, before it crosses over to negative values for $B > 6$ T. Such a positive MR has also been previously observed at low temperature in, e.g.,

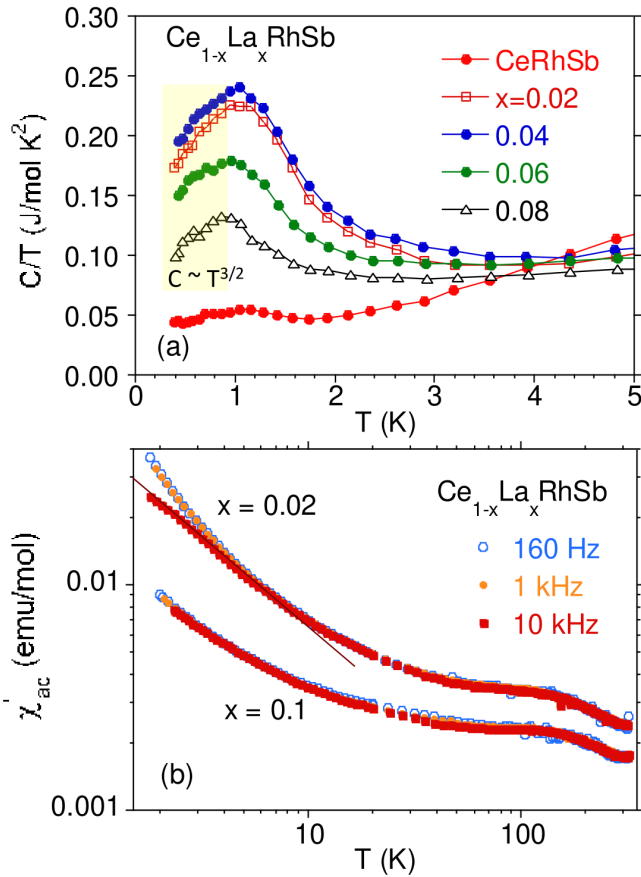


FIG. 11. Temperature dependence of the specific heat divided by temperature, C/T , for $\text{Ce}_{1-x}\text{La}_x\text{RhSb}$ (a). Panel (b) shows the ac susceptibility χ' vs T , at various frequencies.

CeCu_2Si_2 and CeAl_3 heavy fermions, and was discussed as effect coming from the quantum coherent nature of these Kondo lattices. On the other hand, the sign change in the magnetoresistance at around 6 T indicates a disruption of the coherence and is also characteristic feature of the Kondo lattice in the presence of local atomic disorder in the vicinity of Ce ions. The negative magnetoresistance of CeRhSb at the fields higher than 6 T can be associated with the emergence of the local $4f$ magnetic moments. Okawa [53] explained this field induced phenomena theoretically. He calculated the change of the low-temperature MR_T isotherms from their positive to negative value as a result of the presence of local defects around the Ce ions, since local Kondo temperatures are very sensitive to the atomic surrounding of the $4f$ ions. Within this theoretical approach the distribution of the Kondo temperature leads to positive magnetoresistance at low fields, but negative MR at high fields, as shown in Fig. 12. For temperatures $T > 2$ K crossover from positive to negative value of MR is expected for CeRhSb at much substantially higher field than 6 T, as illustrated in Fig. 12. (ii) Two interesting features of the MR isotherms at 2 K appear at $B = 2$ T and 6 T with

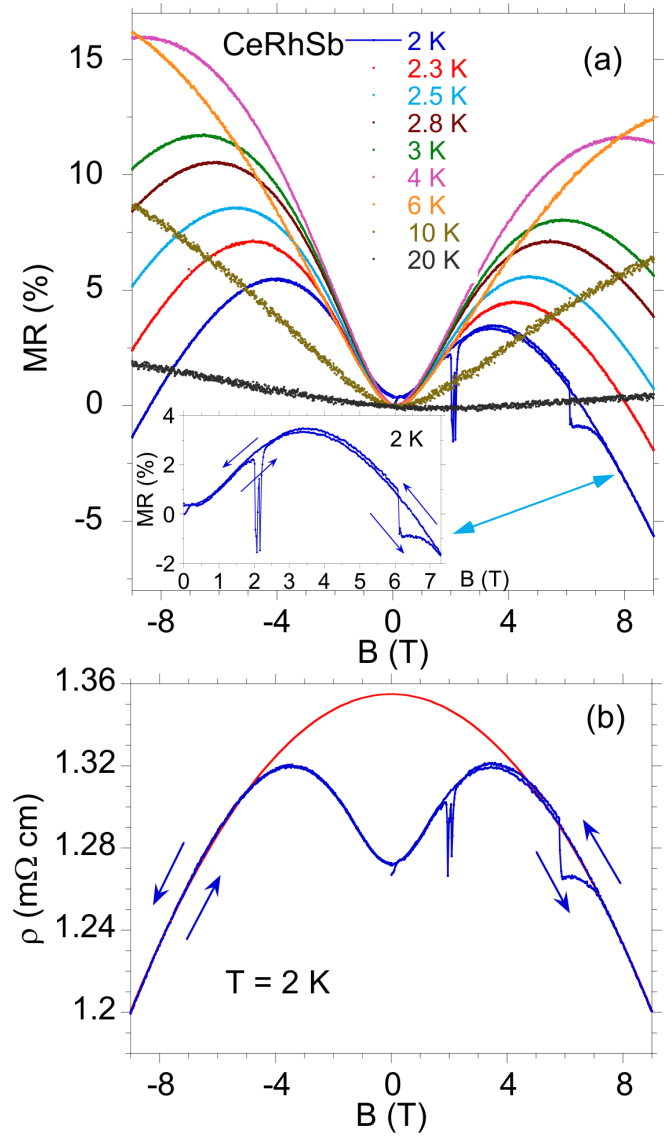


FIG. 12. Magnetoresistance $MR = [\rho(B) - \rho(B = 0)]/\rho(B = 0) \times 100\%$, of CeRhSb (sample thickness was 0.5 mm) as a function of the magnetic field, B , measured at several temperatures (a). The arrows indicate field sweep directions. Magnetic field sequence was $(0 \rightarrow 9 \rightarrow -9 \rightarrow 0)$ T. Inset displays details for 2 K MR isotherm in the positive magnetic fields between 0 and 7 T. Panel (b) shows resistivity ρ vs B of CeRhSb at 2 K measured for the same sample, however twice as thin (sample thickness was 0.5 mm). The field dependence of ρ with negative magnetoresistance effect presented in panel (a) can be well fitted with the expression $\rho = \rho_0 + mB^2$, $m < 0$ (red line).

the increasing field sweep direction, which disappear in the run of field change in the remaining sequence of the measurement cycle ($9 \rightarrow -9 \rightarrow 0$) T. These anomalies disappear at temperature higher than 2 K, as displayed in Fig. 12. Note, these field induced anomalies are reproducible in repeated cycles of measurements of the MR_{2K} isotherm after cooling the sample. Nevertheless, only in

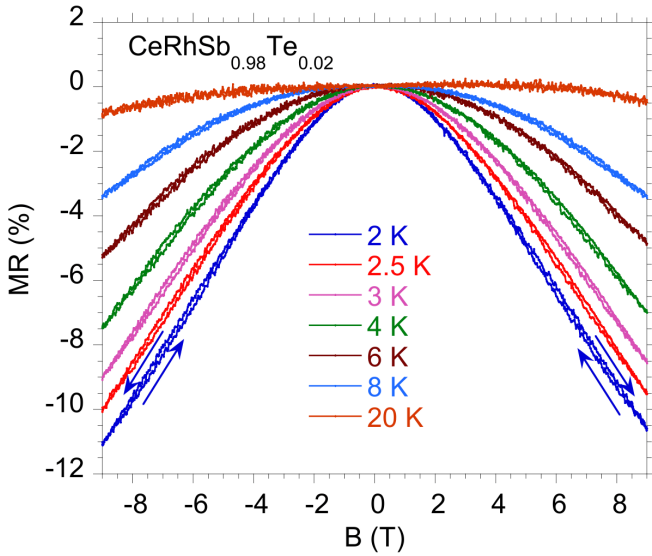


FIG. 13. Magnetoresistance $MR = [\rho(B) - \rho(B = 0)] / \rho(B = 0) \times 100\%$, of $\text{CeRhSb}_{0.98}\text{Te}_{0.02}$ as a function of B , measured at several temperatures. The arrows indicate field sweep directions. Magnetic field sequence was $(0 \rightarrow 9 \rightarrow -9 \rightarrow 0)$ T (sample thickness was 0.5 mm).

the runs with the increasing field. In general, doped both CeRhSb and CeNiSn are disordered systems with a random anisotropy and competing interparticle interactions. Then, magnetic nanoparticles can be formed. There are known examples of Ce-Kondo lattices, doped with non-magnetic transition elements [54], produce a specific local electronic environment around the Ce ions. In effect, the exchange interactions between the nearest Ce ions depend on the random occupation in the vicinity of each of them and even could lead to a spin-glass-like state at low temperature [so-called nonmagnetic atom disorder (NMAD) spin glass state [55]]. In a very diluted system, i.e., where the number of defects is small and the interparticle dipole-dipole interactions are negligibly small in comparison with anisotropy energy, the low temperature anomalous phenomena, attributed to dynamics of weakly magnetic nanoparticles, can be explained by superparamagnetic framework of the Néel-Brown model [56, 57]. Within the model, the flipping rate τ for the nanomagnetic particle is $\tau = \tau_0 \exp(-KV/k_B T)$, where τ_0 is a microscopic relaxation time in the order of $(10^{-9} - 10^{-13})$ s, K is the anisotropy constant, and V is the volume of particle. When $KV \gg k_B T$, the magnetic moment is frozen, that is the spin flipping is blocked [58]. The blocking behavior is displayed in Fig. 12 at the field 2.05 T, 2.17 T, and 6.12 T, and corresponds to nanoparticles with frequency $\nu = 1/\tau_0 = 7.3 \times 10^{10} \text{ s}^{-1}$, $7.7 \times 10^{10} \text{ s}^{-1}$, and $21.8 \times 10^{10} \text{ s}^{-1}$, respectively (assuming also that each magnetic cluster has moment of $1 \mu_B$). A probable scenario assumes blocking of nanoparticles with larger volume first and then the smaller next with the increasing B , whereas under larger fields, the particles are oriented with B providing a negative MR behavior. (iii)

Figure 13 exhibits MR vs B for $\text{CeRhSb}_{0.98}\text{Te}_{0.02}$ at selected temperatures. The MR_T isotherms have negative values at all fields and exhibit a weak hysteresis loops between ~ 4 T and ~ 8 T for $T < 6$ K. However, in this situation, the fluctuating nanoparticle moments are not correlated with each other. The component χ'_{ac} shown in Fig. 14 does not depend on ν , while χ''_{ac} shows a strong frequency dependence, different than that, measured for $\text{Ce}_{0.98}\text{La}_{0.02}\text{RhSb}$, characteristic of spin-glass-like phase (cf. Fig. 3). The scenario with noninteract-

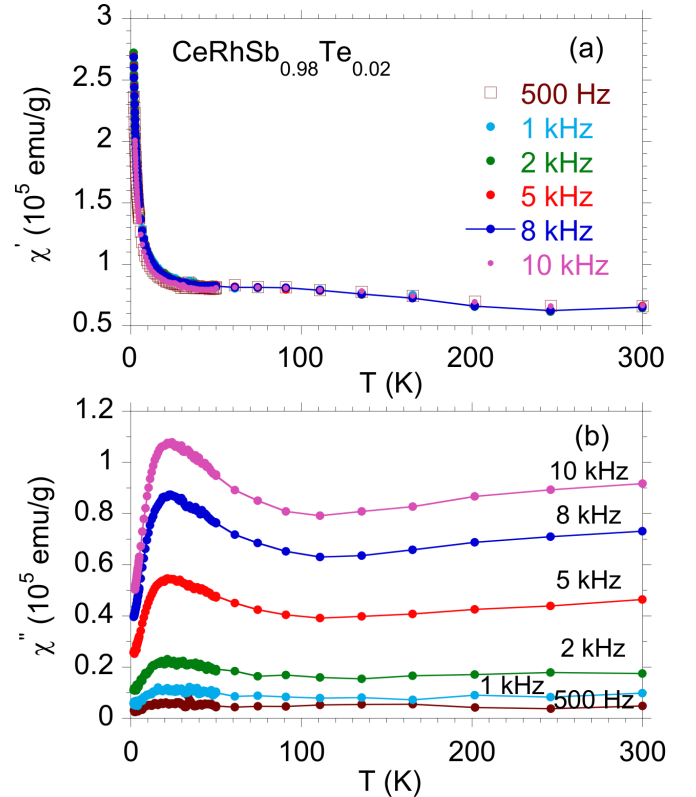


FIG. 14. Temperature dependencies of the real χ' (a) and imaginary χ'' (b) components of the ac mass magnetic susceptibility under magnetic field with amplitude of 2 G.

ing weakly magnetic nanoparticles in $\text{CeRhSb}_{0.98}\text{Te}_{0.02}$ correlates well with the observation of non-Fermi-liquid $\chi \sim C/T \sim T^{-1+\lambda}$ T -dependencies, related to the presence of Griffiths phase in these materials. (iv) In Fig. 12 the various MR_T isotherms measured for 1 mm thick sample under positive fields, are asymmetric in comparison to respective MR_T curves obtained in opposite-sign field. The effect is due to the distribution of the electric field between the electrodes and depends on the thickness of the sample. This is because for the sample of 0.5 mm thick the magnetoresistance at 2 K is fully symmetric under positive and negative fields. Moreover, the magnetic field dependence of the negative magnetoresistance can be fitted accurately by the expression $\rho(B) = \rho(0) + mB^2$, $m < 0$. Figure 13 shows a fully symmetric field dependence of MR_T isotherms for $\text{CeRhSb}_{0.98}\text{Te}_{0.02}$ sample

of thickness of ~ 0.5 mm. A negative magnetoresistance magnitude is increasing with decreasing temperature. To interpret the MR isotherms shown in Figs. 12 and 13, we suggest the following scenario. It has been previously predicted that CeRhSb and CeNiSn could be novel Kondo systems possessing the so-called Möbius-twisted surface states (MKI) [15]. According to high resolution photoemission spectroscopy measurements [59, 60], the both systems can be considered to be semimetallic with an anisotropic hybridization pseudogap. Thus, CeRhSb and CeNiSn are sometime called *failed Kondo insulators*. The resistivity of CeRhSb exhibits a tendency to saturate at $T \rightarrow 0$, as illustrated in Fig. 2. A pronounced saturation effect was also detected for CeNiSn [26, 61] (the saturation of ρ within the gap range is evidently documented for the off-stoichiometric CeNiSn [27]). The ARPES experiment [18] did not confirm unequivocally Möbius topological surface states, predicted for MKI CeRhSb for (010) surface, but it has not been ruled out completely. A. Burkov [62] presented a microscopic model of diffusive magnetotransport in Weyl metals and has thus clarified its relation to the chiral anomaly. Namely, he showed that a measurable consequence of chiral magnetic effect (CME) is a positive magnetoconductivity, proportional to B^2 in the limit of weak magnetic field. In consequence, Weyl metals possess quadratic negative magnetoresistance, which could dominate over other contributions, as was documented experimentally for various topological materials (see, e.g., Refs. [63–65]). In summary, we suggest that the magnetoresistance properties of CeRhSb analyzed here may serve as evidence of the topologically nontrivial nature of this compound. Furthermore, the negative magnetoresistance at 2 K with a bell-shaped profile strongly supports the emergence of the chiral anomaly in CeRhSb, as well as in CeRhSb_{0.98}Te_{0.02}, helping to rationalize the origin of the MR (cf., Figs. 12 and 13).

IV. OUTLOOK

In this paper, we have tested first the robustness of selected universal properties of Kondo insulators against the formation of defects and substitutional doping of systems based on CeRhSb as the initial narrow-gap non-magnetic semiconductor. In this respect, we tested the proposed by us original scaling $\chi\rho = const.$ and have discussed its limitations. Second, we have observed the onset of inhomogeneous magnetic state appearing in the doped system CeRhSb_{1-x}Te_x connected with the increased carrier concentration. The magnetic properties of the last compound provide clear evidence for a breakdown of the collective spin-singlet states with the minute doping. This feature obscures the pure Kondo insulating behavior as evidenced through the observed magnetic and electric (magneto)resistance behavior as a function of either temperature or applied magnetic field. The collected data concerning the new temperature and

applied magnetic field scaling are summarized in Table I. On the basis of those scalings suggestions concerning the topological character of their states are made.

V. ACKNOWLEDGMENTS

J.S. acknowledges the support from Narodowe Centrum Nauki, Grants OPUS No. UMO-2018/29/B/ST3/02646 and No. UMO-2021/41/B/ST3/04070.

Appendix A: Anderson–Kondo model for deriving the magnetic susceptibility

The temperature dependence of magnetic susceptibility has been derived starting from Anderson–Kondo lattice Hamiltonian in the strong correlation limit, which has the form

$$\begin{aligned} \mathcal{H} = & \hat{\mathcal{P}} \left\{ \sum_{mn\sigma} t_{mn} \hat{c}_{m\sigma}^\dagger \hat{c}_{n\sigma} + \sum_{im\sigma} \frac{2|V_{im}|^2}{U + \epsilon_f} \frac{\hat{v}_{if\bar{\sigma}}}{4} \right\} \hat{\mathcal{P}} \quad (\text{A1}) \\ & + \hat{\mathcal{P}} \left\{ \sum_{i\sigma} \epsilon_f \hat{v}_{if\sigma} + \sum_{im\sigma} (V_{im} \hat{f}^\dagger \hat{c}_{m\sigma}) + \text{H.c.} \right\} \hat{\mathcal{P}} \\ & + \hat{\mathcal{P}} \left\{ \sum_{im} \frac{2|V_{im}|^2}{U + \epsilon_f} \left(\hat{\mathbf{S}}_i \cdot \hat{\mathbf{s}}_m - \frac{\hat{v}_{if} \hat{n}_m}{4} \right) \right\} \hat{\mathcal{P}} \\ & + \hat{\mathcal{P}} \left\{ -\frac{1}{2} g_f \mu_B H \sum_{i\sigma} \sigma \hat{N}_{i\sigma} - \frac{1}{2} g_c \mu_B H \sum_{m\sigma} \sigma \hat{n}_{m\sigma} \right\} \hat{\mathcal{P}} \\ & + \hat{\mathcal{P}} \left\{ \sum_{ij} J_{ij} \left(\hat{\mathbf{S}}_i \cdot \hat{\mathbf{S}}_j - \frac{\hat{v}_{if} \hat{v}_{jf}}{4} \right) \right\} \hat{\mathcal{P}}. \end{aligned}$$

In this Hamiltonian, the projection operators $\hat{\mathcal{P}}$ exclude double f -orbital occupancies. The consecutive terms are: The first represents the effective hopping between conduction–electron (c) sites (m, n) with t_{mn} being the bare hopping amplitude, V_{im} is the hybridization amplitude between c and f electrons. The second is composed of spin-flip assistant c -electron hopping ($\hat{\mathbf{S}}_i$ is the f -electron spin operator) and the bare atomic f -level position ϵ_f . The third term represents the projected hybridization part. The fourth and the sixth terms represent the Kondo ($\tilde{V}^2/(U + \epsilon_f)$) and f exchange ($\tilde{V}^4/(U + \epsilon_f)^3$) parts, respectively. The fifth term represents the Zeeman energy in the static applied field H for f and c electrons, respectively. Finally, U is the interatomic $f-f$ Coulomb coupling. In general, this type of Hamiltonian takes into account Kondo ($f-c$) and superexchange interactions in an explicit form in addition to the intraatomic correlation. Such a starting point matches well with the subsequent solution which accounts accurately only for intraatomic correlations.

This Hamiltonian is solved in the statistically consistent Gutzwiller–approximation (SGA), in which the effective single–particle Hamiltonian takes the form,

$$\begin{aligned}
\mathcal{H}_{MF} = & - \sum_{\langle mn \rangle \sigma} (\nu(\hat{c}_{m\sigma}^\dagger \hat{c}_{n\sigma} - \zeta) + \text{H.c.}) \quad (\text{A2}) \\
& - \lambda_{cm} \sum_{m\sigma} (\sigma(\hat{c}_{m\sigma}^\dagger \hat{c}_{m\sigma} - m_c)) \\
& - \mu \sum_{i\sigma} (\hat{c}_{i\sigma}^\dagger \hat{c}_{i\sigma} + \hat{f}_{i\sigma}^\dagger \hat{f}_{i\sigma}) \\
& - \sum_{i\sigma} (\tau_\sigma(\hat{f}_{i\sigma}^\dagger \hat{f}_{i\sigma} - m_f)) \\
& - \lambda \sum_{i\sigma} (\hat{f}_{i\sigma}^\dagger \hat{f}_{i\sigma} + \hat{c}_{i\sigma}^\dagger \hat{c}_{i\sigma} - n_e) + \langle \mathcal{H} \rangle,
\end{aligned}$$

where the variational parameters $\nu, \lambda_{cm}, \lambda_f, \lambda$, and the chemical potential μ , are all determined variationally so that the statistical consistency is obeyed. For details of this cumbersome analysis see. [32, 66] In the approach, the average $\langle \mathcal{H} \rangle$ is approximated in such a manner that the effective mean–field Hamiltonian \mathcal{H}_{mf} of single–particle form, with a number of effective fields to be evaluated through a self–consistent procedure, involving simultaneous solution up to 12 integral equations in the most general case.

-
- [1] G. Aeppli and Z. Fisk, *Comments Condens. Matter Phys.* **16**, 155 (1992).
- [2] T. Ekino, T. Takabatake, H. Tanaka, and H. Fujii, *Phys. Rev. Lett.* **75**, 4262 (1995).
- [3] J. Spałek, *Acta Phys. Pol. A* **97**, 71 (2000).
- [4] T. Takabatake, Y. Nakazawa, M. Ishikawa, T. Sakakibara, K. Koga, and I. Oguro, *J. Magn. Magn. Mater.* **77-76**, 87 (1988).
- [5] A. Ślebarski, A. Jezierski, A. Zygmunt, S. Mähl, and M. Neumann, *Phys. Rev. B* **58**, 13498 (1998).
- [6] A. Ślebarski, A. Jezierski, A. Zygmunt, S. Mähl, M. Neumann, and G. Borstel, *Phys. Rev. B* **54**, 13551 (1996).
- [7] M. Dzero, K. Sun, V. Galitski, and P. Coleman, *Phys. Rev. Lett.* **104**, 106408 (2010).
- [8] M. Dzero, K. Sun, P. Coleman, and V. Galitski, *Phys. Rev. B* **85**, 045130 (2012).
- [9] M. Neupane, N. Alidoust, S-Y. Xu, T. Kondo, Y. Ishida, D. J. Kim, Chang Liu, I. Belopolski, Y. J. Jo, T-R. Chang, H-T. Jeng, T. Durakiewicz, L. Balicas, H. Lin, A. Bansil, S. Shin, Z. Fisk, and M. Z. Hasan, *Nat. Commun.* **4**, 3991 (2013).
- [10] N. Xu, X. Shi, P. K. Biswas, C. E. Matt, R. S. Dhaka, Y. Huang, N. C. Plumb, M. Radović, J. H. Dil, E. Pomjakushina, K. Conder, A. Amato, Z. Salman, D. McK. Paul, J. Mesot, H. Ding, and M. Shi, *Phys. Rev. B* **88**, 121102(R) (2013).
- [11] J. Jiang, S. Li, T. Zhang, Z. Sun, F. Chen, Z.R. Ye, M. Xu, Q.Q. Ge, S.Y. Tan, X.H. Niu, M. Xia, B.P. Xie, Y.F. Li, X.H. Chen, H.H. Wen, and D.L. Feng, *Nat. Commun.* **4**, 4010 (2013).
- [12] S. Wolgast, Ç. Kurdak, K. Sun, J. W. Allen, Dae-Jeong Kim, and Z. Fisk, *Phys. Rev. B* **88**, 180405(R) (2013).
- [13] D. J. Kim, S. Thomas, T. Grant, J. Botimer, Z. Fisk, and Jing Xia, *Sci. Rep.* **3**, 3150 (2013).
- [14] D. J. Kim, J. Xia, and Z. Fisk, *Nat. Mater.* **13**, 466 (2014).
- [15] P. -Y. Chang, O. Erten, and P. Coleman, *Nat. Phys.* **13**, 794 (2017).
- [16] T.-S. Nam, Chang-Jong Kang, D.-C. Ryu, Junwon Kim, Heejung Kim, Kyoo Kim, and B. I. Min, *Phys. Rev. B* **99**, 125115 (2019).
- [17] G. Nakamoto, T. Takabatake, H. Fujii, A. Minami, K. Maezawa, I. Oguro, and A. A. Menovsky, *J. Phys. Soc. Jpn.* **64**, 4834 (1995).
- [18] Seungho Seong, Kyoo Kim, Eunsook Lee, Chang-Jong Kang, Taesik Nam, B. I. Min, Takenobu Yoshino, T. Takabatake, J. D. Denlinger, and J.-S. Kang, *Phys. Rev. B* **100**, 035121 (2019).
- [19] S. K. Malik and D. T. Adroja, *Phys. Rev. B* **43**, 6295 (1991).
- [20] A. Ślebarski, *J. Alloys Compd.* **423**, 15 (2006).
- [21] A. Ślebarski, M. B. Maple, E. J. Freeman, C. Sirvent, M. Radłowska, A. Jezierski, E. Granado, Q. Huang and J. W. Lynn, *Phil. Mag.* **82**, 943 (2002).
- [22] B. H. Toby, *Powder Diffr.* **21**, 67 (2006).
- [23] A. Ślebarski, J. Spałek, M. Fijałkowski, J. Goraus, T. Cichorek, and Ł. Bochenek, *Phys. Rev. B* **82**, 235106 (2010).
- [24] A. Ślebarski and J. Spałek, *Phys. Rev. Lett.* **95**, 046402 (2005).
- [25] J. Spałek, A. Ślebarski, J. Goraus, L. Spałek, K. Tomala, A. Zarzycki, and A. Hackemer, *Phys. Rev. B* **72**, 155112 (2005); A. Ślebarski, J. Spałek, M. Gamża, and A. Hackemer, *Phys. Rev. B* **73**, 205115 (2006).
- [26] A. Ślebarski, M.B. Maple, R.E. Baumbach, and T.A. Sayles, *Phys. Rev. B* **77**, 245133 (2008).
- [27] A. Ślebarski A and J. Spałek, *Phil. Mag.* **89**, 1845 (2009).
- [28] J. Spałek and A. Ślebarski, *J. Phys.: Conf. Ser.* **273**, 012055 (2011).
- [29] M. F. Hundley, P. C. Canfield, J. D. Thompson, Z. Fisk, and J. M. Lawrence, *Phys. Rev. B* **42**, 6842 (1990).
- [30] V. Jaccarino, G. K. Wertheim, J. H. Wernick, L. R. Walker, and A. Sigurd, *Phys. Rev.* **160**, 476 (1967); G. Aeppli and Z. Fisk, *Comments Condens. Matter Phys.* **16**, 155 (1992).
- [31] T. Takabatake, T. Yoshino, H. Tanaka, Y. Bando, H. Fujii, T. Fujita, H. Shida, and T. Suzuki, *Physica B* **206-207**, 804 (1995).
- [32] O. Howczak, Ph.D. thesis, Jagiellonian University, Kraków 2012, https://th-www.if.uj.edu.pl/ztns/download/phdTheses/0lga_Howczak_doktorat.png
- [33] S. K. Malik, L. Menon, K. Ghosh, and S. Ramakrishnan *Phys. Rev. B* **51**, 399 (1995).
- [34] D. T. Adroja, B. D. Rainford, A. J. Neville, P. Mandel,

- and A. G. M. Jansen, *J. Magn. Magn. Mater.* **161**, 157 (1996).
- [35] J. S. Kim, E.-W. Scheidt, D. Mixson, B. Andraka, and G. R. Stewart, *Phys. Rev. B* **67**, 184401 (2003).
- [36] L. Menon, F. E. Kayzel, A. de Visser, and S. K. Malik, *Phys. Rev. B* **58**, 85 (1998).
- [37] A. Ślebarski and J. Goraus, *Phys. Stat. Solidi B* **247**, 710 (2010).
- [38] R. Doradziński and J. Spalek, *Phys. Rev. B* **56**, R14239 (1997); *Phys. Rev. B* **58**, 3293 (1998); for brief review see: J. Spalek and R. Doradziński, *Acta Phys. Polon. A* **96**, 677 (1999); *ibid.* **97**, 71 (2000).
- [39] P. W. Anderson, *Phys. Rev.* **124**, 41 (1961).
- [40] O. Gunnarsson and K. Schönhammer, *Phys. Rev. B* **28**, 4315 (1983); J.C. Fuggle, F.U. Hillebrecht, Z. Zolnierok, R. Lässer, Ch. Freiburg, O. Gunnarsson, and K. Schönhammer, *Phys. Rev. B*, **27**, 7330 (1983).
- [41] A. H. Castro Neto, G. Castilla, and B. A. Jones *Phys. Rev. Lett.* **81**, 3531 (1998).
- [42] A. H. Castro Neto and B. A. Jones *Phys. Rev. B* **62**, 14975 (2000).
- [43] P. Hean, J. Flouquet, F. Lappierre, P. Lejay, and G. Remenyi, *J. Low Temp. Phys.* **67**, 391 (1987).
- [44] R. Sollie and P. Schlottmann, *J. Appl. Phys.* **69**, 5478 (1991).
- [45] R. Sollie and P. Schlottmann, *J. Appl. Phys.* **70**, 5803 (1991).
- [46] P. Schlottmann, *Phys. Rev. B* **54**, 12324 (1996).
- [47] J. M. D. Coey, S. vMolnar, and R. J. Gambino, *Solid State Commun.* **24**, 167 (1977).
- [48] L. Menon and S. K. Malik, *Physica B* **230-232**, 695 (1997).
- [49] T. Yoshino, T. Takabatake, M. Sera, M. Hiroi, N. Takamoto, and K. Kindo, *J. Phys. Soc. Jpn.* **67**, 2610 (1998).
- [50] D. T. Adroja and B. D. Rainford, *J. Magn. Magn. Mater.* **135**, 333 (1994).
- [51] Y. Uwatoko, G. Oomi, S. K. Malik, T. Takabatake, and H. Fujii, *Physica B* **199-200**, 572 (1994).
- [52] S. K. Malik, L. Menon, V. K. Pecharsky, and K. A. Gschneidner, *Phys. Rev. B* **55**, 11471 (1997).
- [53] F. J. Ohkawa, *Phys. Rev. Lett.* **64**, 2300 (1990).
- [54] A. Ślebarski, *J. Alloys Compd.* **480**, 9 (2009).
- [55] K. A. Gschneidner Jr., J. Tang, S. K. Dhar, and A. Goldman, *Physica B* **163**, 507 (1990).
- [56] L. Néel, *Ann. Geophys. (C.N.R.S.)* **5**, 99 (1949).
- [57] W. F. Brown, Jr., *Phys. Rev.* **130**, 1677 (1963).
- [58] At high temperatures, the moment flipping between two directions of its easy axis is described by superparamagnetism.
- [59] H. Kumigashira, T. Takahashi, S. Yoshii, and M. Kasaya *Phys. Rev. Lett.* **87**, 067206 (2001).
- [60] K. Shimada, K. Kobayashi, T. Narimura, P. Baltzer, H. Namatame, M. Taniguchi, T. Suemitsu, T. Sasakawa, and T. Takabatake, *Phys. Rev. B* **66**, 155202 (2002).
- [61] T. Takabatake, M. Nagasawa, H. Fujii, G. Kido, M. No-hara, S. Nishigori, T. Suzuki, T. Fujita, R. Helfrich, U. Ahlheim, K. Fraas, C. Geibel, and F. Steglich, *Phys. Rev. B* **45**, 5740 (1992).
- [62] A. A. Burkov, *Phys. Rev. B* **91**, 245157 (2015).
- [63] Y. Cui, Y. Chu, Z. Pan, Y. Xing, S. Huang, and H. Xu, *Nanoscale*, **13**, 20417 (2021).
- [64] J. C. de Boer, D. P. Leusink, and A. Brinkman, *J. Phys. Commun.* **3**, 115021 (2019).
- [65] M. Hirschberger¹, S. Kushwaha, Z. Wang, Q. Gibson, S. Liang, C. A. Belvin¹, B. A. Bernevig, R. J. Cava, and N. P. Ong, *Nature Materials* **15**, 1161 (2016).
- [66] O. Howczak and J. Spalek *J. Phys.: Condens. Matter* **24**, 205602 (2012)